Gas-Induced Formation of Cu Nanoparticle as Catalyst for High-Purity Straight and Helical Carbon Nanofibers

Xian Jian,[†] Man Jiang,[†] Zuowan Zhou,[†,*] Qun Zeng,[‡] Jun Lu,[†] Dingchuan Wang,[†] Junting Zhu,[†] Jihua Gou,[§,*] Yong Wang,[†] David Hui,[⊥] and Mingli Yang[‡,*]

[†]Key Laboratory of Advanced Technologies of Materials (Ministry of Education), School of Materials Science and Engineering, Southwest Jiaotong University, Chengdu 610031, China, [‡]Institute of Atomic and Molecular Physics, Sichuan University, Chengdu 610065, China, [§]Department of Mechanical, Materials and Aerospace Engineering, University of Central Florida, Orlando, Florida 32816, United States, and [⊥]Department of Mechanical Engineering, University of New Orleans, New Orleans, Louisiana 70148, United States

ABSTRACT The facile preparation of high-purity carbon nanofibers (CNFs) remains challenging due to the high complexity and low controllability in reaction. A novel approach using gas-induced formation of Cu crystals to control the growth of CNFs is developed in this study. By adjusting the atmospheric composition, controllable preparation of Cu nanoparticles (NPs) with specific size and shape is achieved, and they are further used as a catalyst for the growth of straight or helical CNFs with good selectivity and high yield. The preparation of Cu NPs and the formation of CNFs are completed by a one-step process. The inducing effect of N_2, Ar, H_2, and C_2H_2 on the formation of Cu NPs is systematically investigated through a combined experimental and computational approach. The morphology of CNFs obtained under different conditions is rationalized in terms of Cu NP and CNF growth models. The results suggest that the shapes of CNFs, namely, straight or helical, depend closely on the size, shape, and facet activity of Cu NPs, while such a gas-inducing method offers a simple way to control the formation of Cu NPs.

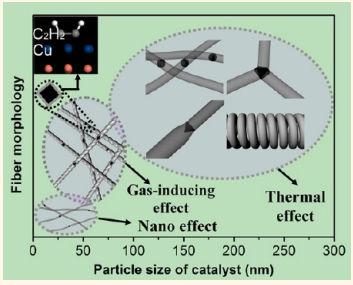

KEYWORDS: carbon nanofibers · Cu nanocrystal · catalyst · gas-inducing method · helical · shape control

Carbon materials can be synthesized in various forms, such as fullerene,[1,2] fiber,[3,4] tubes,[5] graphene,[6] and graphyne.[7] Since the discovery of helical nano- or microcarbon tubes and fibers,[8,9] significant attention has been paid to these specific structures.[10−12] Benefited from their helical characteristics in morphology, coiled carbon fibers/tubes display remarkable elasticity, mechanical strength, chirality, and electromagnetic properties that could offer significant potential in electromagnetic wave absorbers,[13−15] microactuators,[16,17] mechanical components,[18] *etc.* The performances of the coiled carbon fibers/tubes are usually determined by their morphology and geometry,[19] and the control of the structure of the coiled carbon fibers/tubes is essentially important in their preparation. However, the controllable syntheses of these materials have not been fully achieved so far partly due to a lack of understanding of their growth mechanism[20−24] and how it can be adjusted.

Helical carbon species are usually prepared by catalytic chemical vapor deposition (CCVD) from organic substances such as acetylene[25] and methane[26] over Ni,[27] Fe,[28] Sn,[29] or their alloys[30] at high temperatures (>425 °C). A small amount of sulfur or phosphorus impurity and/or H_2, Ar, and N_2 dilute gas is required during these reactions.[25] In these methods, the yield, purity, and helicity of the synthesized carbon materials depend on the catalyst, carbon source, reaction temperature, gas-flow rate, substrate, *etc.* It has been reported that the helical carbon fibers usually grow on the surface of faceted catalyst nanoparticles.[31] Qin *et al.* obtained one kind of amorphous helical carbon nanofibers (HCNFs) at a temperature as low as 195 °C by using Cu nanoparticles (NPs) as the catalyst.[32] Most of the faceted Cu NPs, located at the node of these two coiled fibers, have a rhombic projection.[33] Shaikjee *et al.* reported that Cu particles with a decahedra (asymmetrical) shape favor the growth of helically coiled fibers while trigonal bipyramidal (symmetrical)-shaped Cu particles grow straight fibers exclusively.[34] All of these studies indicate that the shape and size of catalyst particles have significant influence on the morphologies of HCNFs. Therefore, the study of the morphology of NP catalysts is critical for the preparation of helical carbon materials.

Several methods have been developed to produce semiconductor and metal particles in a variety of structures like cubes,[35]

* Address correspondence to zwzhou@at-c.net, jihua.gou@ucf.edu, myang@scu.edu.cn.

Received for review April 29, 2012 and accepted September 10, 2012.

Published online September 10, 2012
10.1021/nn301880w

core−shell[36−38] tetrahexahedrons,[39] and rods,[40] *etc.*, over the past decade.[41,42] In most applications, these NP catalysts are required to retain their high dispersibility in reaction media, preferably in the form of nanocrystals with precisely controlled shapes and sizes. However, the effective size and shape control and agglomeration resistance of the NPs remain a great challenge.

Particular attention has been paid to the gas-inducing approach by which various catalytic NPs were produced in the atmosphere and then used in CNF preparation.[43−51] In this study, we proposed for the first time a modified gas-induced technique that uses C_2H_2, which also serves as carbon source, and its mixture with H_2, N_2, or Ar to realize the *in situ* preparation of high-purity straight or helical CNFs on the formed Cu nanocatalysts from the decomposition of cupric tartrate. The reaction proceeds with good selectivity and high yield. It was found that this method is effective in controlling the size, shape, and growth of Cu NPs used for the preparation of carbon nanofibers. The first-principle study of gas adsorption on the copper surface reveals that the gases have different levels of interaction with Cu facets, which modifies the morphology of Cu NPs and as a consequence affects the formation of straight or helical fibers. The details of this gas-inducing method, such as reaction time, temperature, and substrates (MgO), were studied for an effective control of the formation of CNFs with desired morphology.

RESULTS AND DISCUSSION

Preparation of Straight and Helical Fibers. Cupric tartrate is a usual Cu source in the preparation of Cu crystal. Qin *et al.*[33] reported that the cupric tartrate decomposes into Cu nanocrystals under vacuum, and the as-synthesized Cu grains are effective catalysts for the growth of helical carbon fibers. Instead of the air-free condition, several kinds of atmospheres were introduced during the decomposition of cupric tartrate in our study. It was found that the activity of the formed catalyst particles is highly atmosphere-dependent. Three kinds of atmospheres including N_2, H_2, and C_2H_2 lead to CNFs with different morphologies in a facile process. High-purity and straight CNFs were obtained under N_2, while high-purity and helical CNFs were obtained under C_2H_2. The purity of straight or helical carbon fiber can reach 95%, as shown in Figure 1a,c. Under H_2, thick and straight fibers were formed with a small portion of slender and helical nanofibers (Figure 1b). The morphologies of the three kinds of carbon fibers are shown in Figure 1a−c. In addition to the difference in shape, the straight and helical fibers have significant different diameters, from 150 to 300 nm for the former and about 100 nm for the latter.

The above observations indicate that some physical or chemical interactions exist between the atmosphere and the Cu surface and affect the formation of helical or straight CNFs. In order to obtain Cu nanocrystals with desired size and structure, a technique to prevent the particles from the aggregation and oxidation is required before the CCVD process. In this study, the thermotropic behavior of the catalyst precursor with differential scanning calorimetry (DSC) was first investigated. The DSC curve of the cupric tartrate shows one endothermic peak at 276 °C at a heating rate of 10 °C/min under N_2 (Figure S1 in Supporting Information) but two endothermic peaks at 261.0 and 271.8 °C at 5 °C/min (Figure S2), which are attributed to pyrolytic decomposition of cupric tartrate into metallic copper and tartrate fragments.[52] The exothermic peaks at 283.4 °C in Figure S1 and 294.6 °C in Figure S2 correspond to the combination and crystallization of Cu atoms. It is clear that the heating rate has considerable influence on the Cu nanocrystal formation. Therefore, a heating rate of 3 °C/min and a maximum temperature of 271.8 °C were set for a precise control of Cu crystallization in this study.

The Cu nanocatalysts were then obtained under N_2, H_2, and C_2H_2. Figure 1d shows the environmental scanning electronic microscope (ESEM) image of the copper particles generated under N_2, which exhibit various shapes such as spheres and rods and have an average grain size of about 120 nm. However, the particles obtained under H_2 atmosphere have much smaller diameters of about 50 nm (Figure 1e), and these Cu NPs tend to aggregate with each other in order to reduce their surface energy. The size distribution of the Cu particles produced under N_2 and H_2 was measured from their TEM images with the Nano Measurer[53] program. The results are shown in Figures S3 and S4. The particle size under N_2 ranges from 61.52 to 202.59 nm with an average of 117.91 nm, while the particles under H_2 have a wider size distribution from 18.78 to 374.69 nm and have an average size of 125.50 nm. However, a direct observation to the Cu NPs under C_2H_2 is not applicable since C_2H_2 quickly adsorbs onto the Cu surfaces and polymerizes with each other to form carbon fibers.[31] It is speculated that the "fiber seeds" generated at the initial stage adhere to and coat the Cu NPs and prevent the NPs from further aggregation. To verify this speculation, H_2 was used as a carrier of C_2H_2 to speed the C_2H_2 polymerization. As it is shown in Figure 1f, uniform Cu NPs were obtained from the decomposition of cupric tartrate at 271.8 °C for 10 s under a mixed gas atmosphere (C_2H_2/H_2 = 1/10, flow rate of C_2H_2: 10 mL/min). These Cu NPs have an average size of about 50−80 nm and are dispersed fairly well. We have shown that temperature, gas composition, ratio, and flow rate have considerable influence on the formation of Cu NPs and CNFs. Further studies on these factors would be helpful for a more precise control over the CNF shapes and sizes.

Correlation between Carbon Fibers and Catalyst Particles. Further analysis was conducted to understand the relationship between the morphology of carbon fibers

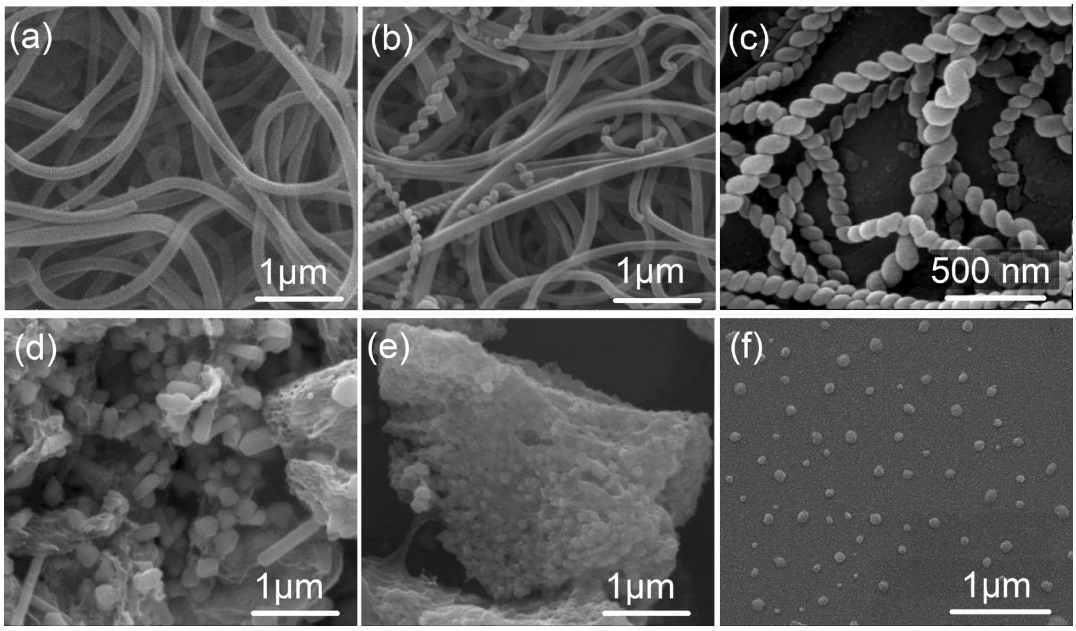

Figure 1. SEM images of three kinds of carbon fibers (a−c) and their corresponding catalyst particles (d−f) obtained from the decomposition of copper tartrate under N_2, H_2, and a mixed gas atmosphere (C_2H_2/H_2 = 1/10) at 271.8 °C, respectively.

and the catalyst particles on which they grow. TEM images of typical straight and helical nanofibers are shown in Figure 2. In Figure 2a, the straight CNFs have a linear structure with diameters of 100−200 nm. The inside catalyst particles are sphere-like with a diameter of 90−180 nm, as shown in Figure 2c. In contrast, the helical nanofibers are more slender than the straight fibers, and the wrapped catalyst particles are polyhedral in most cases (Figure 2b). Most of these faceted particles have different lengths in edge without symmetry in architecture, located in the middle of the helical fibers, as shown in Figure 2d. The particle size is about 20−80 nm. The two branches of the helical fibers are the mirror images of each other, and they exhibit identical cycle numbers, fiber diameters, coil diameters, and coil pitches. Most of the helical fibers have diameters between 50 and 100 nm, whereas the straight fibers usually have larger diameters. The diameters of the two kinds of fibers (straight and helical ones) are approximately equal to the size of the catalyst particle. These results indicate that the morphology of carbon fibers is related to the polygonal nature of the catalyst particles and the fiber diameter is related to the catalyst particle size.

A salient feature of catalyst particles is their shape change during fiber growth,[31,54] which suggests that acetylene has the selectivity during the adsorption on the different facets of Cu particles, making different facets have different growth rates. As a result, a reconstructure of the particles occurs to form more regular structures. Different atmospheres, N_2, H_2, and C_2H_2, tend to have different activities on the Cu surface, which is speculated to govern the differential growth leading to straight or helical CNFs.

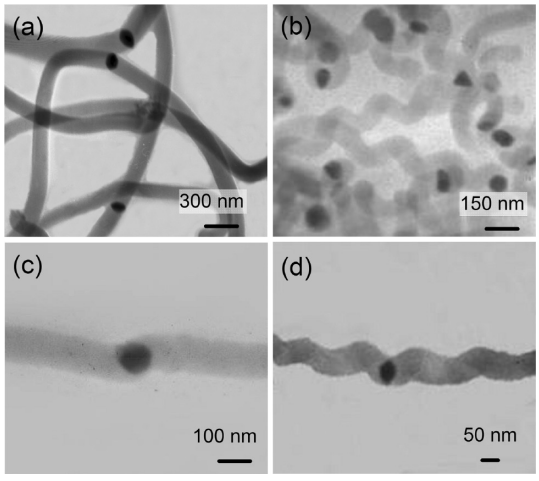

Figure 2. TEM images of typical straight and helical carbon fibers.

First-Principle Study of Gas Adsorption on the Cu Surfaces. To reveal the impetus for the diverse Cu particle growth, we investigated the surface properties of the copper crystals under different atmospheres, in particular, to their surface activity, which is directly related to the particle growing preference, by means of density functional theory (DFT) calculations under the generalized gradient approximation (GGA) of Perdew and Wang,[55] as implemented in the DMol^3 package.[56] Four gases, namely, Ar, N_2, H_2, and C_2H_2, were selected for the purpose of comparison.

The selected four gases exhibit quite different adsorption behavior. The equilibrium distances of Ar from the closest Cu atoms are 4.16, 4.15, and 4.01 Å in the low-index (100), (110), and (111) surfaces, respectively, indicating a rather weak interaction between Ar

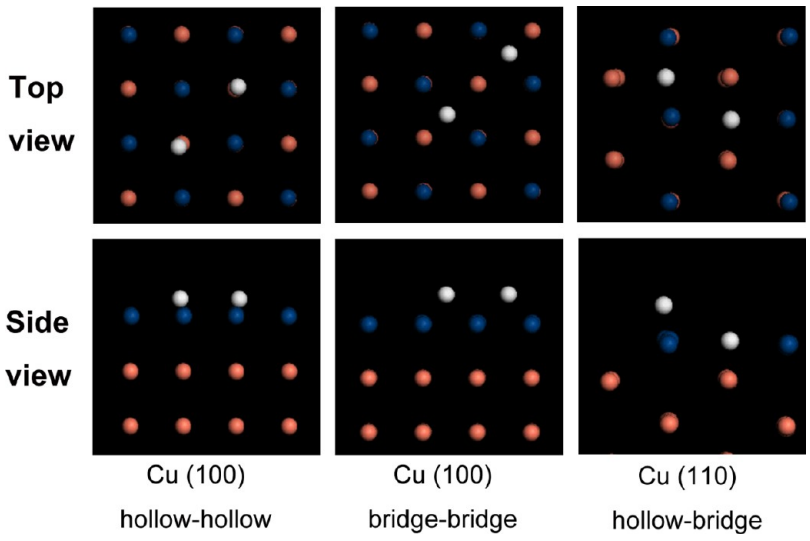

Figure 3. Optimal adsorption sites of H_2 molecule on Cu(100), (110), and (111) surfaces. Cu atoms are denoted in blue (the first layer) and red (internal layers). H atoms are in white.

and the crystal surfaces (Figure S5). N_2 has a similar behavior with Ar, molecularly kept away from all three surfaces with the N−N distances of 3.48, 3.43, and 3.77 Å, respectively (Figure S6). The corresponding N−Cu distances are 1.10, 1.10, and 1.11 Å, indicating a very weak interaction of N_2 on the crystal surface. Therefore, both Ar and N_2 stay far away from the Cu surfaces. It can be assumed that the atmosphere of Ar and N_2 has very little effect on the Cu NPs growth under normal atmosphere.

In contrast, H_2 is adsorbed dissociatively on the Cu(100) and (110) surfaces, while it remains in its molecular form on the (111) surfaces, resulting from the mismatch between the H−H bond length and Cu−Cu distance on the (111) surface. There are three possible adsorption sites for H_2: atop, bridge, and hollow on these three surfaces. However, the atop adsorption was found to be much less stable than the other two. Three kinds of energetically favorable geometries of H_2 on the (100) and (110) surfaces including bridge−bridge (BB), bridge−hollow (BH), and hollow−hollow (HH) were identified, as shown in Figure 3. In all three patterns, H_2 is basically parallel to the surface and the H−H distances are 2.87, 2.97, and 2.71 Å. They are much longer than 0.75 Å, which is the bond length of free H_2 at the same level. The corresponding Cu−H distances are 0.79, 0.99, and 1.08 Å, respectively, indicating a strong bonding between the H atom and the surface. Affected by the H_2 chemisorption, the Cu−Cu distances near the adsorption sites are subjected to some changes of about $-0.09 \sim +0.17$ Å. The most favorable structure is the BH geometry found on the (110) surface, which is 0.16 and 0.01 eV more stable than the BB and HH, respectively. Therefore, the H_2 adsorption is strong enough to change the surface activity of Cu NPs and as a consequence to affect the growth along the corresponding facets.

Acetylene on the low-index Cu facets is either molecularly or dissociatively adsorbed, as shown in Figure 4. Five energetically favorable conformations of C_2H_2 on the Cu surface were identified. Four of them are two-fold hollow (TFH) adsorption, while the rest are four-fold hollow (FFH) adsorption. In all cases, Cu bonds with C atoms and makes C_2H_2 bent or dissociated. Three of the four TFH patterns (Figure 4a−d) are molecular adsorption. In the three patterns, the C−C axis is almost parallel to the copper surface, and the carbon atoms are 1.28−2.19 Å above the copper layer. The H−C−C bond angles change from 180 to 148.72 and 140.00° on (111), to 119.81 and 119.76° on (100), to 119.59 and 119.69° on (110). The C−C bond length of the adsorbed C_2H_2 moiety increases to 1.30, 1.37, and 1.35 Å on (111), (100), and (110), respectively. In the last TFH pattern (Figure 4e), C_2H_2 is dissociated with the C−C and C−H distances of 1.25 and 2.92 Å, respectively. The shortest C−Cu distance is 1.91 Å, which is much shorter than those in other patterns. In the FFH adsorption, C_2H_2 binds to four copper atoms with C−C and C−H distances of 1.39 and 1.10 Å.

The interaction between the adsorbate and surface is indicated by its adsorption energy (E_{ad}), which is defined as the energy difference between the adsorbed system and free adsorbate and the surface. Table 1 lists the E_{ad} of the four gases on Cu(111), (100), and (110) surfaces. E_{ad} values are very small for N_2 and Ar but are large for C_2H_2. H_2 has an intermediate E_{ad} value. From these calculations, it can be seen that C_2H_2 has the most strong interaction with the Cu surface, followed by H_2, while N_2 and Ar are inactive. Moreover, H_2 and C_2H_2 have preferences to certain Cu facets. In all of the calculations, the inclusion of dispersion correction[57] increases the E_{ad} value by 11−84% but does not change the E_{ad} order, as shown in Table 1. The PW91 and PBE functionals produce similar E_{ad} values,

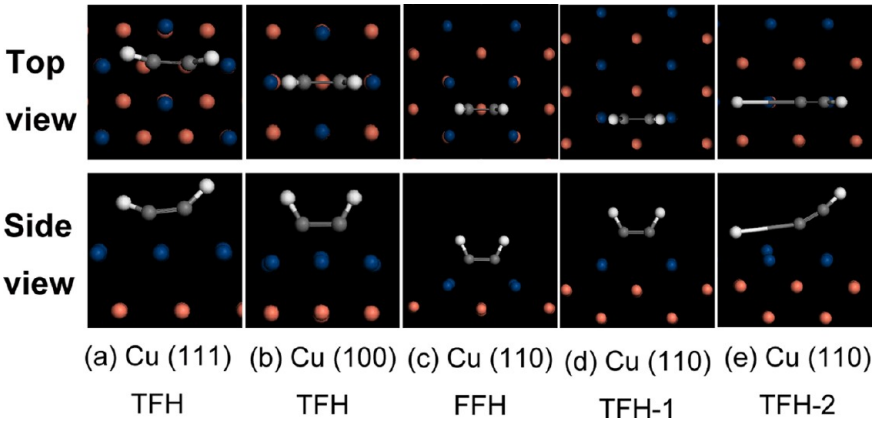

Figure 4. Optimal adsorption sites of acetylene on Cu(100), (110), and (111) surfaces. Cu atoms are denoted by large blue (the first layer) and red (internal layers) balls, C and H atoms are shown in gray and white, respectively.

while BLYP underestimates the E_{ad}. However, the E_{ad} order of these three functionals is essentially the same.

By placing one to four H_2 or C_2H_2 molecules on the Cu surface, the E_{ad} variation with coverage was investigated. The computed results are given in Table S3. The E_{ad} variation depends on the adsorbate, adsorption pattern, and crystal facet. Here we discuss only the strongest adsorption, C_2H_2 on Cu(111), whose E_{ad} values for the second, third, and fourth adsorptions are all positive, indicating that C_2H_2 has the tendency to be adsorbed onto the Cu surfaces successively. In order to model the behaviors of Cu NPs at a very beginning stage, which are very small in size, the adsorption on a Cu_8 cluster was calculated. The Cu_8 structure was taken from our earlier study.[58,59] The adsorption of N_2, Ar, H_2, and C_2H_2 on the Cu_8 cluster at various sites was studied. The four gases have different E_{ad} values, so do the different adsorbing sites on Cu_8 surfaces, as shown in Table S4, revealing that the adsorption is gas- and site-selective for small-sized Cu NPs, which is similar to the bulk case.

Under H_2, C_2H_2, or their mixture, the active sites on the Cu NP facets are dynamically occupied by gas molecules. Since the adsorbates have different preferences toward different facets, the occupancy rates are different from facet to facet. For example, the H_2 favors the adsorption on the (100) and (110) instead of the (111) surfaces, and the BH adsorption on the (110) surface is most favorable, making these surfaces have different occupancy rates under adsorption−desorption equilibrium. The growth of Cu crystals on a surface will be hindered when it is occupied by gas molecules. As a result, the Cu growth may have different rates on the surfaces depending on their adsorbing ability to the gas molecules, which leads to different growth rates on the Cu NP surfaces and results in various shapes of Cu NPs. By this way, the gas component, H_2 or C_2H_2, affects the Cu NPs' growth preference and modifies their morphologies. For example, the small size of C_2H_2- and H_2-induced NPs is attributed to the coverage of gas molecules on Cu surfaces; the shape and size distribution are controlled by adjusting the gas composition since the adsorption is related to the partial pressures of gas components.

TABLE 1. Computed Adsorption Energies (E_{ad}) of N_2, Ar, H_2, and C_2H_2 on the Cu Facets[a]

		E_{ad}/eV				
system	adsorption sites	PW91	PW91+D	PBE	PBE+D	BLYP
C_2H_2/Cu(111)	TFH	1.63	1.98	1.65	1.94	0.73
C_2H_2/Cu(100)	TFH	1.36	1.89	1.54	2.26	0.50
C_2H_2/Cu(110)	TFH-1	0.77	1.29	0.99	1.96	0.55
C_2H_2/Cu(110)	TFH-2	0.94	1.06	0.76	1.58	0.36
C_2H_2/Cu(110)	FFH	0.97	1.71	1.39	2.92	0.70
H_2/Cu(110)	BH	0.23	0.40	0.25	1.01	0.13
H_2/Cu(100)	HH	0.22	0.60	0.42	1.46	0.22
H_2/Cu(100)	BB	0.07	0.44	0.26	1.42	0.13
N_2/Cu(100)	H	0.04	0.22	0.12	0.71	0.05
N_2/Cu(110)	B	0.09	0.18	0.08	0.12	0.01
N_2/Cu(111)	H	0.07	0.18	0.07	0.62	0.02
Ar/Cu(100)	TFH	0.08	0.26	0.17	0.78	0.00
Ar/Cu(110)	TFH	0.13	0.18	0.11	0.04	0.05
Ar/Cu(111)	TFH	0.10	0.18	0.10	0.37	0.01

[a] $E_{ad} = E_{gas} + E_{surf} - E_{gas/surf}$.

Adjustment to Reaction Conditions. The growth of carbon materials depends not only on the catalyst but also on the reaction conditions. Several factors that affect the morphologies of carbon fibers were identified. The reaction time for Cu nanocrystal formation, which starts from the decomposition of cupric tartrate until C_2H_2 injection, definitely affects the size and topography of the formed Cu NPs. Longer reaction time promotes larger-size NPs. By extending the reaction time from 30 min to 2 h, larger-size Cu NPs (>1 μm, Figures S8 and S9) were obtained than those shown in Figure 1d. Using these large-size NPs as catalysts, the obtained fibers are mostly in straight and thick form, confirming the above mechanism that the size and morphology determine the fiber shapes.

The substrate also has influence on the NP size by preventing the NPs from the aggregation. By carefully

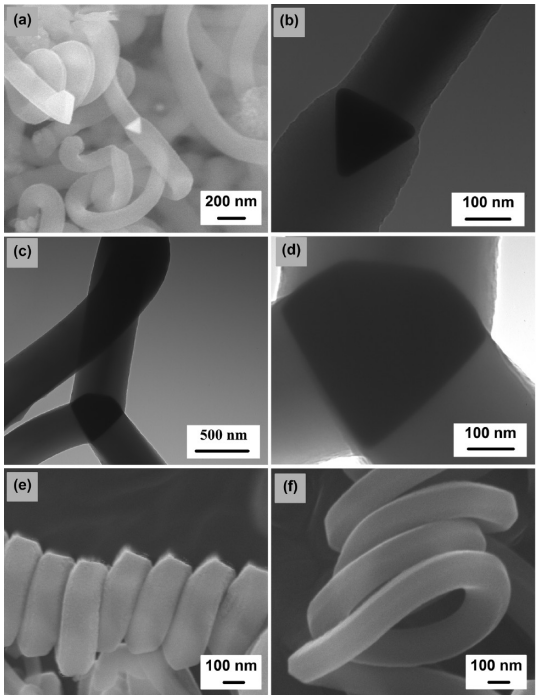

Figure 5. Morphologies of the three special fibers prepared at 300 °C for 60 min under N_2. SEM (a) and TEM (b) images of the straight fiber with different fiber diameters. (c) TEM and (d) images of the fibers with trident structure. (e) SEM and (f) images of fibers possessing the structure of submicro helix with coil diameters of (e) 500 nm and (f) 975 nm.

selecting the substrate, for example, MgO, Al_2O_3, *etc.*, a very small size of NPs can be obtained. The substrate effect on the CNF formation has been studied by several researchers.[60,61] To lower their surface energy, the small-sized NPs tend to adopt spherical structures[58,59] and exhibit catalytic isotropy, resulting in the formation of curved fibers. In this study, smaller Cu particles were obtained on a MgO substrate (MgO/cupric tartrate = 3:1) and *in situ* applied to the CNF growth. Curved fibers (Figure S10) about 20 nm in diameter were produced, while the wrapped Cu particles are spherical in shape and less than 20 nm in size, as shown in the HRTEM image (Figure S11).

In addition, another three types of fibers, neither straight nor helical, were found at higher temperature of 300 °C. The first one has a jump, where a Cu NP sits within the diameter along the fiber direction, as shown in Figure 5a,b. The thicker branch grows on the surface with larger area, while the thinner grows on the side with smaller area. The second one is the fiber with a trident structure (Figure 5c,d), which has the similar morphology with the previously identified Y-shaped and tripod-like carbon fibers.[62,63] The third one is a submicro helix, whose diameter is larger than 100 nm, as shown in Figure 5e,f. These submicro structures originate from NPs with large facet area. These three structures account for about 2, 3, and 8% among the common straight fibers, respectively, as analyzed from the SEM image in Figure S12. Our observations on morphologies of Cu NPs and

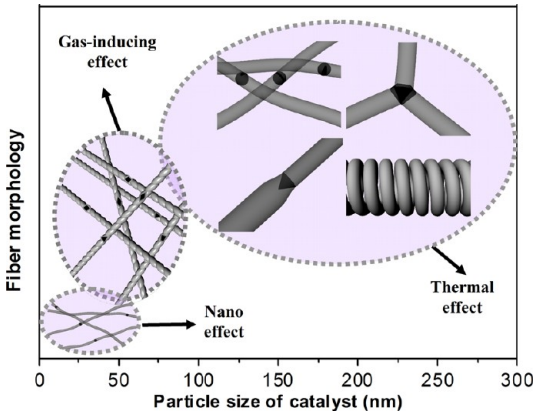

Figure 6. Interplay among gas-inducing, thermal, and size effects on the formation of carbon fibers.

CNFs suggest a close correlation between the NP structures and the fibers growing on them, although the details of this correlation are not fully revealed.

In summary, Cu particles, atmosphere composition, and synthetic temperature are the main aspects in the growth control of CNFs. Figure 6 shows a schematic diagram that describes the dependence of CNF morphology on the Cu NP size. With increasing particle size, the formed CNFs have a series of changes in morphology. On the basis of the experimental and computational results, we found that three effects are relevant to the CNF growth. The first is "nano effect", which is dominant when the Cu NPs are smaller than 20 nm. Because of their large surface area, the particles tend to adopt spherical structures on which thin and curved CNFs grow. Between 20 and 100 nm, the particle shapes are related to the atmosphere under which either straight or helical CNFs can be prepared depending on the atmosphere composition. The size distribution of NPs is closely related to the reaction temperature. The Cu NPs aggregate quickly and grow into large Cu nanoparticles (>100 nm) with regular shapes at high temperatures (300 °C or higher). These regular particles have large facets in favor of the formation of straight and thick fibers. Therefore, the adjustment of NP size distribution and reaction temperature is the key to atmosphere induction technique for high-purity straight or helical CNF preparation.

CONCLUSIONS AND OUTLOOK

A gas-inducing method was developed to achieve the controllable preparation of straight and helical carbon nanofibers. First, the Cu NPs with specific size and shape were produced under atmospheres of N_2, H_2, Ar, and/or C_2H_2. A direct correlation of the structure and surface reactivity of Cu NPs with atmospheric composition was observed and revealed by density functional theory calculations. Second, the straight or helical high-purity CNFs catalyzed by the Cu NPs were prepared under facile reaction conditions. The morphology of CNFs highly depends on the size, shape, and surface reactivity of the Cu NPs. As a result,

the CNFs with specific morphology can be controllably prepared by adjusting the atmospheric composition.

This newly developed gas-inducing method not only has advantages to carbon fiber synthesis but also finds its way to potential application in the preparation of metal nanocrystals with desired morphology. In a preliminary study, cubic and rod-like Cu NPs (Figure S13) were successfully produced using a similar approach. It is inspiring that this gas-inducing method opens a new gate to control the morphology of NPs.

METHODS

Experimental Procedures. The Cu NPs in question generated from the decomposition of cupric tartrate were prepared from potassium sodium tartrate and copper(II) chloride with a precipitation method.[52,64] The fabrication of the nanofiber was carried out at atmospheric pressure in a quartz tube (45 mm in diameter and 1300 mm in length), which was set into a horizontal furnace and heated at a specific rate of less than 3 °C/min. A ceramic boat paved with a thin layer of the catalyst precursor was placed into the center of the reaction tube. The heating continued until the catalyst precursor was decomposed into copper particles at 271.8 °C under atmosphere of nitrogen, hydrogen, acetylene, or mixtures thereof. Then, acetylene was introduced into the tube to form the nanofiber. The morphologies of the catalyst particles and the fibril samples were observed using an environmental scanning electron microscope (ESEM, Fei, Quanta 200) and a field emission scanning electron microscope (FESEM, Fei, Inspect-F), both with an accelerating voltage of 20 kV. Meanwhile, the catalyst particle embedded in the middle of the nanofiber was investigated employing transmission electron microscopy (TEM, H-700H) at an accelerating voltage of 160 kV.

Computational Details. The quantum chemical calculations were performed using the Materials Studio Dmol^3 version 4.1 packages (Accelrys, San Diego, CA). These calculations employed a GGA-type Perdew–Wang exchange-correlation functional (GGA-PW91)[55] and a double numeric polarization (DNP) basis set with effective core potentials. Two more functionals, PBE and BLYP, were also used for comparison. Dispersion effect was included in the PW91 and PBE calculations. The basis set superposition error correction was applied to all of the adsorption energies. The surface was treated with the slab model, in which the neighboring surfaces are separated by 15 Å of vacuum. A supercell of $2 \times 2 \times 4$ (4 layers of substrate), and fine mesh points were chosen. A standard value of 4.4 Å is assigned to be the cutoff radius. No symmetry constraint was imposed during geometry optimization.

Conflict of Interest: The authors declare no competing financial interest.

Acknowledgment. This work was financially supported by the National Natural Science Foundation of China (Nos. 90305003, 91016002, and 51173148), the Special Research Fund for Doctoral Program of Higher Education (No. 20060613004), the NBRP (Grant No. 2011CB606200), and the Fundamental Research Funds for the Central Universities (No. 2010XS31 and No. SWJTU11ZT10). The discussion with Dr. Y. Qin in the Max Planck Institute of Microstructure Physics, Germany, is gratefully acknowledged. All authors thank the reviewers for their helpful comments and suggestions.

Supporting Information Available: Figures S1–S13 and Tables S1–S4. Additional details and information on the preparation and characterization of catalyst precursor (DSC/TG analysis), catalyst particles (TEM, SEM snapshots, and XRD patterns), and carbon fibers (TEM, SEM snapshots). Simulations results of C_2H_2, H_2, N_2, and Ar on Cu surfaces and Cu_8 cluster. This material is available free of charge *via* the Internet at http://pubs.acs.org.

REFERENCES AND NOTES

1. Maggini, M.; Scorrano, G.; Prato, M. Addition of Azomethine Ylides to C_{60}: Synthesis, Characterization, and Functionalization of Fullerene Pyrrolidines. *J. Am. Chem. Soc.* **1993**, *115*, 9798–9799.
2. Accorsi, G.; Armaroli, N. Taking Advantage of the Electronic Excited States of [60]-Fullerenes. *J. Phys. Chem. C* **2010**, *114*, 1385–1403.
3. Lawrence, J. G.; Berhan, L. M.; Nadarajah, A. Elastic Properties and Morphology of Individual Carbon Nanofibers. *ACS Nano* **2008**, *2*, 1230–1236.
4. Shaikjee, A.; Coville, N. J. A Novel Type of Carbon: The Synthesis of Patterned Co-block Carbon Nanofibers. *Small* **2011**, *7*, 2593–2597.
5. Liu, J.; Rinzler, A.; Dai, H.; Hafner, J.; Bradley, R.; Boul, P.; Lu, A.; Iverson, T.; Shelimov, K.; Huffman, C. Fullerene Pipes. *Science* **1998**, *280*, 1253–1256.
6. Geim, A. K.; Novoselov, K. S. The Rise of Graphene. *Nat. Mater.* **2007**, *6*, 183–191.
7. Malko, D.; Neiss, C.; Viñes, F.; Görling, A. Competition for Graphene: Graphynes with Direction-Dependent Dirac Cones. *Phys. Rev. Lett.* **2012**, *108*, 086801.
8. Davis, W. R.; Slawson, R. J.; Rigby, G. R. An Unusual Form of Carbon. *Nature* **1953**, *171*, 756–756.
9. Zhang, X.; Zhang, X.; Bernaerts, D.; Tendeloo, G. V.; Amelinckx, S.; Landuyt, J. V.; Ivanov, V.; Nagy, J.; Lambin, P.; Lucas, A. The Texture of Catalytically Grown Coil-Shaped Carbon Nanotubules. *Europhys. Lett.* **1994**, *27*, 141–146.
10. Tang, N.; Wen, J.; Zhang, Y.; Liu, F.; Lin, K.; Du, Y. Helical Carbon Nanotubes: Catalytic Particle Size-Dependent Growth and Magnetic Properties. *ACS Nano* **2010**, *4*, 241–250.
11. Liu, W. C.; Lin, H. K.; Chen, Y. L.; Lee, C. Y.; Chiu, H. T. Growth of Carbon Nanocoils from K and Ag Cooperative Bicatalyst Assisted Thermal Decomposition of Acetylene. *ACS Nano* **2010**, *4*, 4149–4157.
12. Zhao, M. Q.; Zhang, Q.; Tian, G. L.; Huang, J. Q.; Wei, F. Space Confinement and Rotation Stress Induced Self-Organization of Double-Helix Nanostructure: A Nanotube Twist with a Moving Catalyst Head. *ACS Nano* **2012**, *6*, 4520–4529.
13. Motojima, S.; Hoshiya, S.; Hishikawa, Y. Electromagnetic Wave Absorption Properties of Carbon Microcoils/PMMA Composite Beads in W Bands. *Carbon* **2003**, *41*, 2658–2660.
14. Xie, G.; Wang, Z.; Cui, Z.; Shi, Y. Ni-Fe-Co-P Coatings on Coiled Carbon Nanofibers. *Carbon* **2005**, *43*, 3181–3183.
15. Tang, N.; Yang, Y.; Lin, K.; Zhong, W.; Au, C.; Du, Y. Synthesis of Plait-like Carbon Nanocoils in Ultrahigh Yield, and Their Microwave Absorption Properties. *J. Phys. Chem. C* **2008**, *112*, 10061–10067.
16. Li, C.; Thostenson, E. T.; Chou, T. W. Sensors and Actuators Based on Carbon Nanotubes and Their Composites: A Review. *Compos. Sci. Technol.* **2008**, *68*, 1227–1249.
17. Bell, D.; Sun, Y.; Zhang, L.; Dong, L.; Nelson, B.; Grutzmacher, D. Three-Dimensional Nanosprings for Electromechanical Sensors. *Sens. Actuators, A* **2006**, *130*, 54–61.
18. Chen, X.; Zhang, S.; Dikin, D. A.; Ding, W.; Ruoff, R. S.; Pan, L.; Nakayama, Y. Mechanics of a Carbon Nanocoil. *Nano Lett.* **2003**, *3*, 1299–1304.
19. Chen, X.; Motojima, S.; Iwanga, H. Vapor Phase Preparation of Super-Elastic Carbon Micro-coils. *J. Cryst. Growth* **2002**, *237–239*, 1931–1936.
20. Amelinckx, S.; Zhang, X.; Bernaerts, D.; Zhang, X.; Ivanov, V.; Nagy, J. A Formation Mechanism for Catalytically Grown Helix-Shaped Graphite Nanotubes. *Science* **1994**, *265*, 635–639.
21. Kuzuya, C.; In-Hwang, W.; Hirako, S.; Hishikawa, Y.; Motojima, S. Preparation, Morphology, and Growth Mechanism of Carbon Nanocoils. *Chem. Vapor. Depos.* **2002**, *8*, 57–62.
22. Pan, L.; Zhang, M.; Nakayama, Y. Growth Mechanism of Carbon Nanocoils. *J. Appl. Phys.* **2002**, *91*, 10058–10061.

23. Lu, M.; Li, H. L.; Lau, K. T. Formation and Growth Mechanism of Dissimilar Coiled Carbon Nanotubes by Reduced-Pressure Catalytic Chemical Vapor Deposition. *J. Phys. Chem. B* **2004**, *108*, 6186–6192.
24. Motojima, S.; Chen, Q. Three-Dimensional Growth Mechanism of Cosmo-Mimetic Carbon Microcoils Obtained by Chemical Vapor Deposition. *J. Appl. Phys.* **1999**, *85*, 3919–3921.
25. Motojima, S.; Kawaguchi, M.; Nozaki, K.; Iwanaga, H. Growth of Regularly Coiled Carbon Filaments by Ni Catalyzed Pyrolysis of Acetylene, and Their Morphology and Extension Characteristics. *Appl. Phys. Lett.* **1990**, *56*, 321–323.
26. Saveliev, A. V.; Merchan-Merchan, W.; Kennedy, L. A. Metal Catalyzed Synthesis of Carbon Nanostructures in an Opposed Flow Methane Oxygen Flame. *Combust. Flame* **2003**, *135*, 27–33.
27. Tang, N.; Kuo, W.; Jeng, C.; Wang, L.; Lin, K.; Du, Y. Coil-in-Coil Carbon Nanocoils: 11 Gram-Scale Synthesis, Single Nanocoil Electrical Properties, and Electrical Contact Improvement. *ACS Nano* **2010**, *4*, 781–788.
28. Qi, X.; Deng, Y.; Zhong, W.; Yang, Y.; Qin, C.; Au, C.; Du, Y. Controllable and Large-Scale Synthesis of Carbon Nanofibers, Bamboo-like Nanotubes, and Chains of Nanospheres over Fe/SnO_2 and Their Microwave-Absorption Properties. *J. Phys. Chem. C* **2010**, *114*, 808–814.
29. Wang, W.; Yang, K.; Gaillard, J.; Bandaru, P.; Rao, A. Rational Synthesis of Helically Coiled Carbon Nanowires and Nanotubes through the Use of Tin and Indium Catalysts. *Adv. Mater.* **2008**, *20*, 179–182.
30. Qi, X.; Zhong, W.; Deng, Y.; Au, C.; Du, Y. Characterization and Magnetic Properties of Helical Carbon Nanotubes and Carbon Nanobelts Synthesized in Acetylene Decomposition over Fe–Cu Nanoparticles at 450 °C. *J. Phys. Chem. C* **2009**, *113*, 15934–15940.
31. Jian, X.; Jiang, M.; Zhou, Z.; Yang, M.; Lu, J.; Hu, S.; Wang, Y.; Hui, D. Preparation of High Purity Helical Carbon Nanofibers by the Catalytic Decomposition of Acetylene and Their Growth Mechanism. *Carbon* **2010**, *48*, 4535–4541.
32. Qin, Y.; Jiang, X.; Cui, Z. Low-Temperature Synthesis of Amorphous Carbon Nanocoils *via* Acetylene Coupling on Copper Nanocrystal Surfaces at 468 K: A Reaction Mechanism Analysis. *J. Phys. Chem. B* **2005**, *109*, 21749–21754.
33. Qin, Y.; Li, H.; Zhang, Z.; Cui, Z. Symmetric and Helical Growth of Polyacetylene Fibers over a Single Copper Crystal Derived from Copper Tartrate Decomposition. *Org. Lett.* **2002**, *4*, 3123–3125.
34. Shaikjee, A.; Franklyn, P. J.; Coville, N. J. The Use of Transmission Electron Microscopy Tomography To Correlate Copper Catalyst Particle Morphology with Carbon Fiber Morphology. *Carbon* **2011**, *49*, 2950–2959.
35. Yu, D.; Yam, V. W. W. Controlled Synthesis of Monodisperse Silver Nanocubes in Water. *J. Am. Chem. Soc.* **2004**, *126*, 13200–13201.
36. Lu, C. L.; Prasad, K. S.; Wu, H. L.; Ho, J. A.; Huang, M. H. Au Nanocube-Directed Fabrication of Au–Pd Core–Shell Nanocrystals with Tetrahexahedral, Concave Octahedral, and Octahedral Structures and Their Electrocatalytic Activity. *J. Am. Chem. Soc.* **2010**, *132*, 14546–14553.
37. Radi, A.; Pradhan, D.; Sohn, Y.; Leung, K. T. Nanoscale Shape and Size Control of Cubic, Cuboctahedral, and Octahedral Cu–Cu_2O Core–Shell Nanoparticles on Si(100) by One-Step, Templateless, Capping-Agent-Free Electrodeposition. *ACS Nano* **2010**, *4*, 1553–1560.
38. Jin, M.; Zhang, H.; Wang, J.; Zhong, X.; Lu, N.; Li, Z.; Xie, Z.; Kim, M. J.; Xia, Y. Copper Can Still Be Epitaxially Deposited on Palladium Nanocrystals To Generate Core–Shell Nanocubes Despite Their Large Lattice Mismatch. *ACS Nano* **2012**, *6*, 2566–2573.
39. Tian, N.; Zhou, Z. Y.; Sun, S. G.; Ding, Y.; Wang, Z. L. Synthesis of Tetrahexahedral Platinum Nanocrystals with High-Index Facets and High Electro-oxidation Activity. *Science* **2007**, *316*, 732–735.
40. Johansen, C. G.; Huang, H.; Lu, T. M. Effects of Three-Dimensional Ehrlich–Schwoebel Barrier on Texture Selection during Cu Nanorod Growth. *Appl. Phys. Lett.* **2007**, *91*, 121914.
41. Xia, Y.; Xiong, Y.; Lim, B.; Skrabalak, S. E. Shape-Controlled Synthesis of Metal Nanocrystals: Simple Chemistry Meets Complex Physics? *Angew. Chem., Int. Ed.* **2009**, *48*, 60–103.
42. Tao, A. R.; Habas, S.; Yang, P. Shape Control of Colloidal Metal Nanocrystals. *Small* **2008**, *4*, 310–325.
43. Hansen, P. L. Atom-Resolved Imaging of Dynamic Shape Changes in Supported Copper Nanocrystals. *Science* **2002**, *295*, 2053–2055.
44. Chen, Q.; Richardson, N. V. Surface Facetting Induced by Adsorbates. *Prog. Surf. Sci.* **2003**, *73*, 59–77.
45. Newton, M. A.; Belver-Coldeira, C.; Martínez-Arias, A.; Fernández-García, M. Dynamic *In Situ* Observation of Rapid Size and Shape Change of Supported Pd Nanoparticles during CO/NO Cycling. *Nat. Mater.* **2007**, *6*, 528–532.
46. Tao, F.; Dag, S.; Wang, L. W.; Liu, Z.; Butcher, D. R.; Bluhm, H.; Salmeron, M.; Somorjai, G. A. Break-Up of Stepped Platinum Catalyst Surfaces by High CO Coverage. *Science* **2010**, *327*, 850–853.
47. McKenna, K. P.; Shluger, A. L. Shaping the Morphology of Gold Nanoparticles by CO Adsorption. *J. Phys. Chem. C* **2007**, *111*, 18848–18852.
48. Kobayashi, H.; Yamauchi, M.; Kitagawa, H.; Kubota, Y.; Kato, K.; Takata, M. Atomic-Level Pd–Pt Alloying and Largely Enhanced Hydrogen-Storage Capacity in Bimetallic Nanoparticles Reconstructed from Core/Shell Structure by a Process of Hydrogen Absorption/Desorption. *J. Am. Chem. Soc.* **2010**, *132*, 5576–5577.
49. Small, M. W.; Sanchez, S. I.; Marinkovic, N. S.; Frenkel, A. I.; Nuzzo, R. G. Influence of Adsorbates on the Electronic Structure, Bond Strain, and Thermal Properties of an Alumina-Supported Pt Catalyst. *ACS Nano* **2012**, *6*, 5583–5595.
50. Shaikjee, A.; Coville, N. J. The Role of the Hydrocarbon Source on the Growth of Carbon Materials. *Carbon* **2012**, *50*, 3376–3398.
51. Zhang, R.; Khalizov, A.; Wang, L.; Hu, M.; Xu, W. Nucleation and Growth of Nanoparticles in the Atmosphere. *Chem. Rev.* **2012**, *112*, 1957–2011.
52. Schmid, R. L.; Felsche, J. Thermal Decomposition of Cu(II)-$(C_4H_4O_6)\cdot 3H_2O$ and Co(II)$(C_4H_4O_6)\cdot 2.5H_2O$. Determination of Mechanism by Means of Simultaneous Thermal Analysis and Mass Spectrometry. *Thermochim. Acta* **1982**, *59*, 105–114.
53. Shi, Y.; Wang, Y.; Wang, D.; Liu, B.; Li, Y.; Wei, L. Synthesis of Hexagonal Prism (La,Ce,Tb)PO_4 Phosphors by Precipitation Method. *Cryst. Growth Des.* **2012**, *12*, 1785–1791.
54. Qin, Y.; Zhang, Z.; Cui, Z. Helical Carbon Nanofibers with a Symmetric Growth Mode. *Carbon* **2004**, *42*, 1917–1922.
55. Perdew, J. P.; Chevary, J. A.; Vosko, S. H.; Jackson, K. A.; Pederson, M. R.; Singh, D. J.; Fiolhais, C. Atoms, Molecules, Solids, and Surfaces: Applications of the Generalized Gradient Approximation for Exchange and Correlation. *Phys. Rev. B* **1992**, *46*, 6671–6687.
56. Delley, B. From Molecules to Solids with the $DMol^3$ Approach. *J. Chem. Phys.* **2000**, *113*, 7756–7764.
57. Grimme, S. Semiempirical GGA-Type Density Functional Constructed with a Long-Range Dispersion Correction. *J. Comput. Chem.* **2006**, *27*, 1787–1799.
58. Yang, M.; Jackson, K. A.; Koehler, C.; Frauenheim, T.; Jellinek, J. Structure and Shape Variations in Intermediate-Size Copper Clusters. *J. Chem. Phys.* **2006**, *124*, 024308.
59. Jiang, M.; Zeng, Q.; Zhang, T.; Yang, M.; Jackson, K. A. Icosahedral to Double-Icosahedral Shape Transition of Copper Clusters. *J. Chem. Phys.* **2012**, *136*, 104501.
60. Shaikjee, A.; Coville, N. J. The Effect of Copper Catalyst Reducibility on Low Temperature Carbon Fiber Synthesis. *Mater. Chem. Phys.* **2011**, *125*, 899–907.
61. Ren, X.; Zhang, H.; Cui, Z. Acetylene Decomposition to Helical Carbon Nanofibers over Supported Copper Catalysts. *Mater. Res. Bull.* **2007**, *42*, 2202–2210.
62. Zhang, Q.; Cui, Z. Synthesis and Characterization of Y-Shaped Carbon Fibers by Chemical Vapor Deposition. *Mater. Lett.* **2009**, *63*, 850–851.

63. Shaikjee, A.; Coville, N. J. Catalyst Restructuring Studies: The Facile Synthesis of Tripod-like Carbon Fibers by the Decomposition of Trichloroethylene. *Mater. Lett.* **2012**, *68*, 273–276.
64. Qin, Y.; Zhang, Z.; Cui, Z. Helical Carbon Nanofibers Prepared by Pyrolysis of Acetylene with a Catalyst Derived from the Decomposition of Copper Tartrate. *Carbon* **2003**, *41*, 3072–3074.